On Optical Trapping: A Deep Dive into the Hidden Relation Between Classical Laws, Laser Power, and their Applications in Microplastic Study

Varun Sunder Rajan[a†]

Dept. of Physics, Simon Fraser University, Burnaby BC

(Dated: April 13, 2023)

[a] lab partner's name: Adrian Schimmer

We investigate the relationship between laser power and trap strength in optical trapping using a high-power diode laser to trap polystyrene microspheres ranging in size from 1-5 μm in an aqueous solution. We use both equipartition and probability distribution methods to determine the trap strength, finding a positive correlation between trap stiffness and laser power. Varying the laser power between 2.92 mW to 109.8 mW allows us to construct trap stiffness curves for each laser power, confirming that a more powerful laser results in a stronger optical trap. We also investigate the potential energy landscape and histogram of particle positions, showing that potential energy is proportional to trap strength for the trapped polystyrene spheres. Our study provides a more comprehensive understanding of the behavior of microparticles in aqueous solutions under the influence of optical trapping, and has practical implications for researchers in various fields.

INTRODUCTION

Optical tweezers, are a tool for manipulating microscopic particles in various fields, including physics, biophysics, and materials science [1–3]. These tools use the momentum transfer of photons to generate a gradient force that pulls small particles to the center of a focused laser beam, with trapping forces ranging up to piconewtons [4]. Optical tweezers have been used to study a wide range of phenomena, including the stretching of DNA [5] and the trapping of coated microspheres [6].

In this study, we aim to investigate the relationship between laser power and trap strength in optical trapping using submicron-sized polystyrene spheres, and explore the effect of laser power on their displacement. Our custom-built optical tweezers configuration utilized a high-powered diode laser to trap the polystyrene spheres in a water medium. We analyze the significance of Brownian motion in the displacement of trapped particles[1, 2, 7], potential energy, trap strength of the particles, and finally study the relationship between trap strengths and laser power [8]. The magnitude of Brownian motion is reliant on the size and mass of particles, as well as the fluid's viscosity [3]. As the size of the trapped particle decreases, the effect of Brownian motion becomes more pronounced [6].

We employ the potential energy-fitting, probability distribution, and equipartition methods of determining trap strength. Both the potential energy and the histogram curves are analyzed to gain further insights into the underlying physics [9, 10]. Finally, we aim to probe the relationships between power and trap strength.

THEORY

Optical trapping experiments involve the use of laser beams to attract small dielectric particles to regions of high light intensity [8]. When a laser beam is focused on a particle, it generates a local intensity maximum, which creates a trap. This trap is formed due to the intensity gradient produced by the focused beam of light, which exerts a restoring force on the particle at the stable trap position.

The behavior of a trapped particle can be predicted using Hooke's law, which describes the particle's motion as governed by a harmonic potential. The potential energy of the trapped particle is derived via the taylor-expansion of Hooke's law, and is subject to the

force constant κ, which determines the trap stiffness, while the displacement of the particle from the center of the trap in the horizontal and vertical directions are denoted by x and y, respectively [11]. The harmonic potential(s) are given by the equations:

$$U_x(x) = \frac{1}{2}\kappa x^2 \tag{1}$$

$$U_y(y) = \frac{1}{2}\kappa y^2 \tag{2}$$

The potential energy, $U_x(x)$ and $U_y(y)$, are subject to the force constant κ while x and y represent the particle's displacement from the center of the trap in the x and y directions, respectively. The force constant scales with laser power and can also be referred to as the trap stiffness.

In statistical mechanics, the distribution of a system's states can be determined based on the amount of energy available. In the case of optically trapped bead systems, the states are represented by the positions of the beads within the harmonic potential well defined by Equation 1. The probability of finding a bead at a particular position can be calculated using the Boltzmann distribution, which takes the form:

$$p(x) = \frac{1}{Z}\exp\left(\frac{-U(x)}{k_B T}\right) = \frac{1}{Z}\exp\left(\frac{-\kappa x^2}{2k_B T}\right) \tag{3}$$

where Z is the partition function, κ is the spring constant from 1, k_B is Boltzmann's constant, and T is the temperature of the experiment. One can write a similar equation for the y-direction probability. We calculate the correlation between the bead's position at time $t = 0$ and at later time t using an autocorrelation function:

$$\langle x(t)x(0)\rangle = \frac{k_B T}{\kappa} e^{\frac{|t|}{\tau_c}} \tag{4}$$

where the correlation time is given by $\tau_c = \omega c^{-1} = \frac{\gamma}{\kappa}$. By solving the equation of motion for a trapped bead in a harmonic potential, we are able to calculate values for various times. The bead positions measured with a significant time interval are non-correlated when $|t| \gg \tau_c$, hence an exponential drop-off is expected to occur. The motion of the trapped particle can be analyzed by breaking down its trajectory into its individual frequency components and determining the amount of power at each frequency [3]. Autocorrelation analysis is an important tool used to investigate the temporal correlation between positions of a trapped

bead in optical trapping experiments. In Equation 4, the degree of correlation between the position of the bead at different times t is measured. It allows researchers to determine the trap strength without introducing unwanted temporal correlations [4, 6], tying into the purpose of our experiment. To calculate the autocorrelation function, the mean is subtracted from the time series data so that the points represent relative displacements from the center. If the points are uncorrelated, the autocorrelation will look like a delta function, centered about zero with fluctuations of order $1/\sqrt{N}$, where N is the number of observations [7].

Equipartition is another statistical method of determining trap strength. According to the equipartition theorem, each quadratic degree of freedom of a particle in a harmonic potential at thermal equilibrium contributes $\frac{1}{2}k_BT$ of energy to the system [7]. This principle can be used to determine trap strength κ. First, we show the kinetic energy contributions and the potential energy averages as follows:

$$\frac{1}{2}m\langle v_x^2\rangle = \frac{1}{2}k_BT \tag{5}$$

$$\frac{1}{2}m\langle v_y^2\rangle = \frac{1}{2}k_BT \tag{6}$$

$$\langle U_x(x)\rangle = \frac{1}{2}\kappa\langle x^2\rangle \tag{7}$$

$$\langle U_y(y)\rangle = \frac{1}{2}\kappa\langle y^2\rangle \tag{8}$$

where m is the mass of the particle, $\langle v_x^2\rangle, \langle x^2\rangle$ are variances for velocity and displacement in the x-direction, respectively, with similar notation for the y- direction. The $\langle\rangle$ denote ensemble averages. This lab concerns itself with the quadratic contribution of displacement due to the potential energy (equations 1 and 2) of the trap in both directions. Thus we have:

$$\frac{1}{2}\kappa\langle x^2\rangle = \frac{1}{2}k_BT \tag{9}$$

$$\frac{1}{2}\kappa\langle y^2\rangle = \frac{1}{2}k_BT \tag{10}$$

Solving for κ and κ:

$$\kappa = \frac{k_B T}{\langle x^2 \rangle} \tag{11}$$

$$\kappa = \frac{k_B T}{\langle y^2 \rangle} \tag{12}$$

Equations 11 and 12, imply that the bead's spatial motion is described by a symmetric gaussian beam profile, which implies that the trap strength should be the same across the two dimensions. Calculating κ via equipartition is calculation through variance, and is considered to be inaccurate. Trapping is most effective when the radius of the bead $R \approx \lambda$, where λ is the laser's wavelength. This process is theorized by the Mie-scattering regime [2] in the limit $R \approx \omega \approx \lambda$, allowing us to use the wavelength of our diode laser. Then, total beam power is derived as a function of trap stiffness to be,

$$\kappa \approx U_0 \omega \approx \frac{\alpha}{4\pi\omega c} P \tag{13}$$

Here P denotes beam power, c is the speed of light and α is the bead dielectric polarizability. ω is the beam waist: which will be set to 658nm.

The scattering of light from a particle can be described by two regimes: the Mie-scattering regime and the Rayleigh regime, depending on the size of the particle relative to the wavelength of the incident light [2]. α is an important factor in determining the behavior of the trapped particle. In the Rayleigh-scattering regime, the polarizability is approximated as:

$$\alpha \approx \frac{n_p^2}{n_0^2} - 1 \tag{14}$$

where n_p and n_0 are the refraction indices for the bead and immersion oil respectively[4, 6]. The Mie-scattering regime occurs when the size of the particle is comparable to the wavelength of the incident light, resulting in strong dependence of the scattered light on the size of the particle, while the Rayleigh regime occurs when the size of the particle is much smaller than the wavelength of the incident light, resulting in weak dependence of the scattered light on the size of the particle. The trapping efficiency and stiffness of the trap are influenced by the regime, and the trap stiffness can be optimized by adjusting the laser beam power and beam waist [4, 6]. The strength of the optical force acting on a trapped

particle is proportional to the gradient of the optical intensity, which is steeper in the Mie-scattering regime than in the Rayleigh regime. We used polystyrene microspheres ranging in size from 1-5 μm, falling within the Mie-scattering regime for our trapping laser [1, 2]. We use equations 13 and 14 to curve fit data at different power values in the short project portion of our experiment.

METHODS

The optical trapping setup consisted of a 658 nm high-powered diode laser, a FLIR-blackfly camera, an optical breadboard, a variable ND filter, a camera filter, a power meter, an oil-immersion objective (100x, NA = 1.25, 160mm), lenses (25mm and 50mm focal lengths), posts, mounts, cage-system parts, a calibration slide, sample-making equipment, and a low-concentration solution of 1-5 μm diameter polystyrene spheres [11]. We selected 3 μm microspheres for optimal trapping and reproducibility, to avoid the effects of inter-particle van der Waal's forces and weak trapping forces.

The configuration included a laser, two mirrors (M1 and M2), a dichroic mirror, a focusing lens (L3), and a microscope (Figure 1). The laser beam traveled along the cage system's central axis, reflected by the mirrors, and passed through the 45°-angled dichroic mirror. Lens L3 focused the laser light 160 mm away from the objective's back aperture, creating a uniformly illuminated red ring. The camera, equipped with a filter to reduce noise, was positioned 160mm behind the objective for image focusing. The gain and exposure settings were 10dB and default, respectively. A pre-programmed LabVIEW application set the frame rate at 66 fps, guiding the project's initial short option selection.

The experimental setup involved pipetting the solutions under a coverslip taped to a lab slide, which was then sealed with clear nail polish and fixed to the microscope stage using magnets. Immersion oil was applied to match the refractive index of the microscope objective with the sample medium. After focusing the beads in the camera using the xyz translation stage, the laser was turned on to begin trapping, with a short-pass filter used to block stray laser light. The focusing lens was adjusted along the rail to align the trap with the microscope's focal plane. Data collection involved tracking the trapped beads using a FLIR camera and LabVIEW software, with parameters such as bead radius, x-center, and y-center recorded in pixels for at least one minute. A calibration slide with 0.01mm

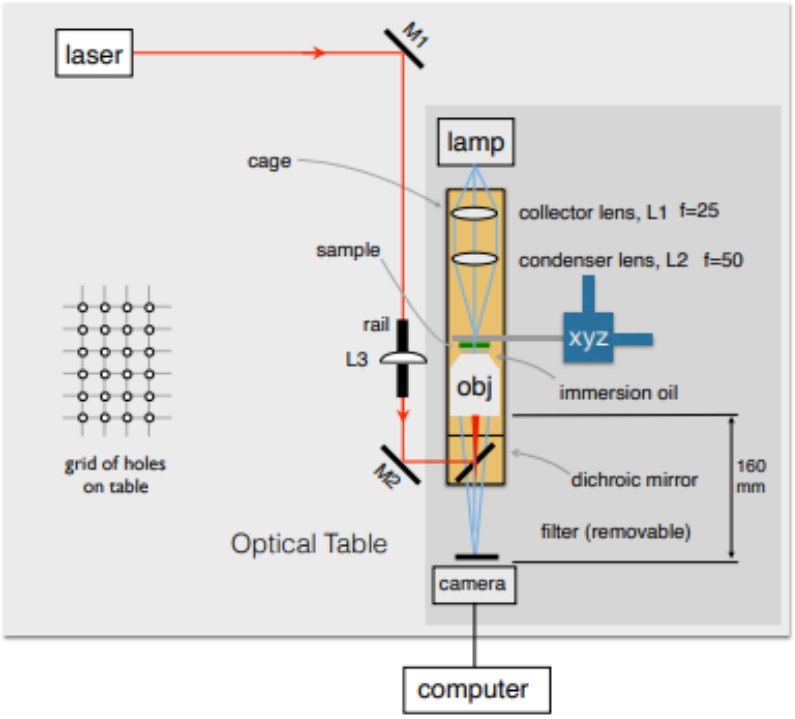

FIG. 1. Schematic diagram of the optical trapping setup.

spacing was used to obtain the pixel to mm conversion, which was found to be $29270 \pm 0.03\%$ pixels per mm. Preprocessing stages involved examining the particle time series for drift, and accounting for noise, which was measured by tracking an empty spot in the trap for noise-correlation.

We obtained the variance of our time-series data, and calculated κ_x and κ_y using the equipartition theorem described from Equations 5 to 12. The trap strength was then calculated via the probability distribution method, where the characteristic Brownian motion allows us to bin the time series and create a histogram, which was fitted to a gaussian distribution. Trap strength was again calculated by binning the time series data according to 3, and fitting it to the potential energy curves 1 and 2, for both the x and y directions. The value ranges for all three methods were compared to each other, and to theory.

To investigate the relationship between laser power and trapping strength, we utilized a variable neutral density (ND) filter and calibrated it by measuring the intensity of the unattenuated laser beam using a power meter. Data collection commenced once a polystyrene sphere was successfully trapped. The trap strength was determined using both the equipartition method and the probability distribution method. We graphed force constants as a

function of laser power, comparing our results with typical values found in the literature. Filter values of -50, -25, 0, 15, and 30 mm were used, with their corresponding power values discussed in the results section. Our methodology aimed to explore the relationship between laser power and trap strength, while accounting for calibration and data preprocessing factors.

RESULTS

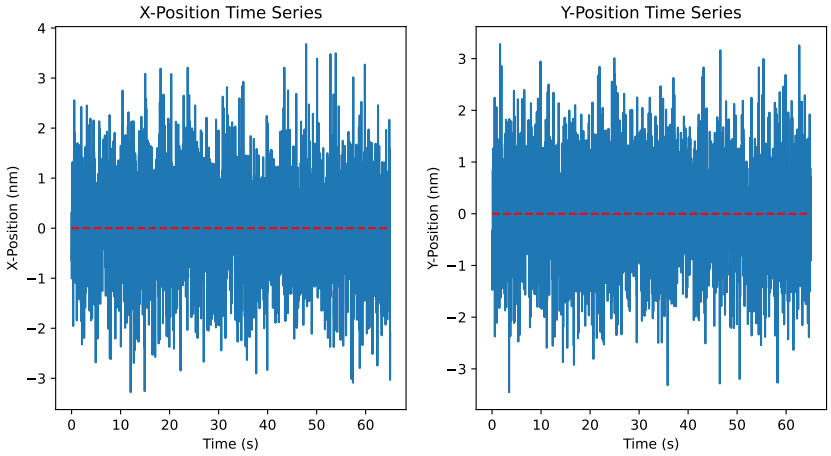

FIG. 2. Time-series plot of Brownian motion showing the displacement of a trapped particle over time in the x and y directions, captured on a 66 frames-per-second FLIR camera. Means are subtracted to normalize data.

Method	κ_x (pN/nm)	κ_y (pN/nm)				
Equipartition	5.71 ±6.94%	2.69 ±15.13%	$\overline{\Delta\%_x}$	4.62%	χ^2_x	14.8
Probability Distribution	5.40 ±6.50%	2.42 ±18.51%	$\overline{\Delta\%_y}$	12.30%	χ^2_y	20.67
Potential Energy	5.24 ±6.49%	2.21 ±18.55%				

TABLE I. Trap stiffness values for all three methods. Percentage discrepancies between the three methods determine precision of measurements with one another. Chi-squared values for x and y respectively indicate deviation from theory. These calculations indicate reasonable precision between experimental methods and deviation from theoretical values. This leads to suspicion surrounding the presence of systematic errors.

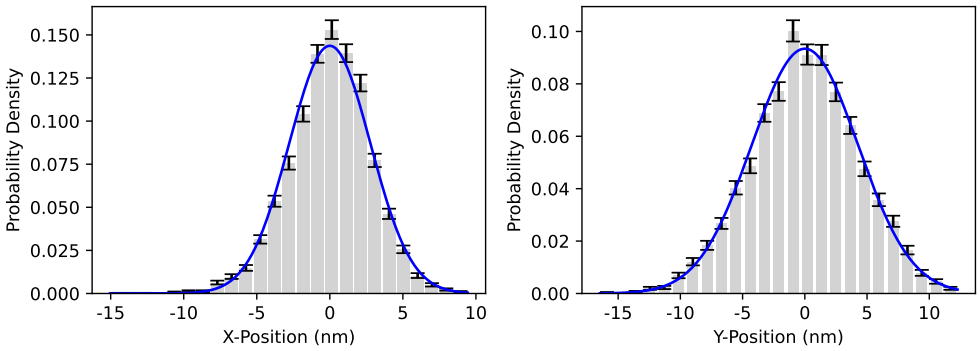

FIG. 3. Histograms of the Brownian motion for the time series data of the particle in both the x and y directions. Gaussians were fitted to histograms to obtain trap strength parameters. Notice the left and right skews for the x and y directions respectively. The calculation of error bars is done by obtaining the square root of the counts per bin and subsequently dividing it by the normalization factor, which is represented by the area beneath the histogram.

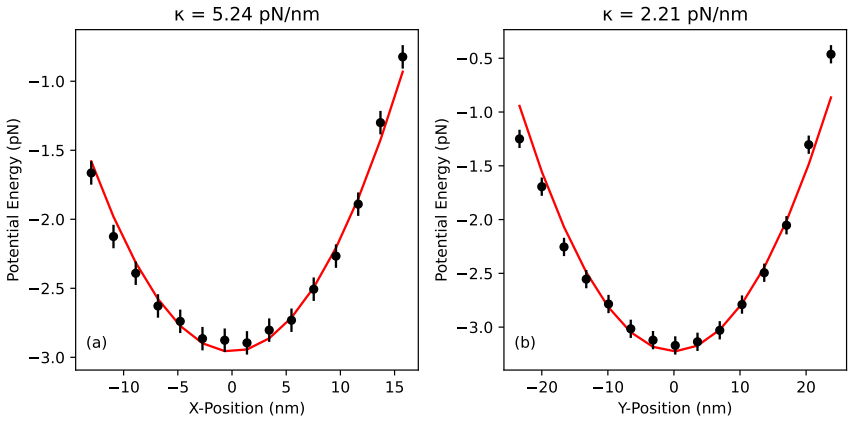

FIG. 4. Data is allotted into 15 bins before plotting the particle's potential energy as a function of position in the x and y directions, using 3. Equations 1 and 2 were then fitted to the binned data to confirm that the states are represented by the position of the bead within the potential well. Error bars were determined by using the time-series data of a particle stuck to the cover-slip as control, setting a foundational point of reference.

Figure 2 displays the time-series data from a specific data set, after subtraction of the mean. We can see the relationship between spatial variance and the equipartition theorem denoted in Equations 11 and 12, obtaining values of: $\kappa_x = 5.71 \pm 6.94\% pN/nm$ and $\kappa_y = 2.69 \pm 15.13\% pN/nm$.

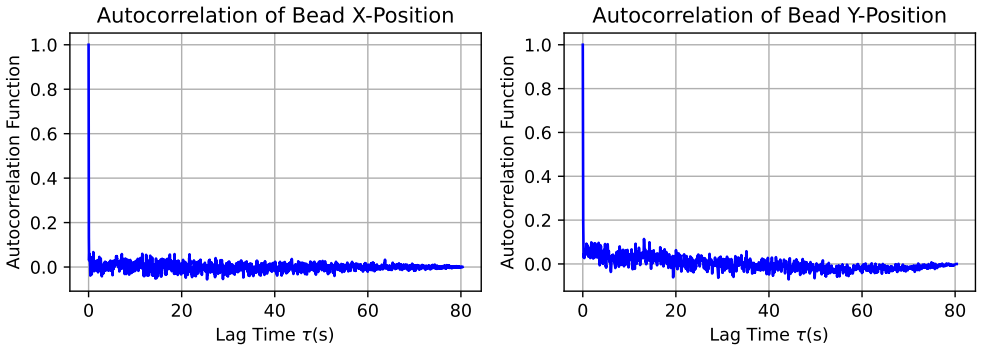

FIG. 5. Auto-correlation functions (ACF) of the Brownian motion time-series, calculated from the x and y displacement data, using Equation 4. The ACF quantifies the correlation between the particle's position at two different time points, and is a measure of the temporal persistence of the motion. The ACF decays exponentially to zero as the time lag increases.

ND filter value (mm)	Power value (mW)
-50	2.92
-25	8.06
0	27.1
15	79.1
30	109.8

TABLE II. ND filter values and corresponding power values

We assessed the trap strength using the probability distribution method discussed in *Theory* and *Methods* (Figure 3), which yielded force constant parameters from the fitted gaussians to be: $5.40 \pm 6.50\% pN/nm$ and $2.42 \pm 18.51\% pN/nm$, for κ_x and κ_y respectively. This falls into expected ranges [10, 12].We note a slight left-skew and right-skew in our respective histograms, which is further pronounced by the fitted gaussians. Possible reasons will be explored in the *Discussion*.

The two potential energy plots in Figure 4 yield the force constants: $\kappa_x = 5.24 \pm 6.49\% pN/nm$ and $\kappa_y = 2.21 \pm 18.55\% pN/nm$ for the x and y directions respectively. The smaller value for κ_y indicates a weaker trap and therefore we expect a wider well, which is consistent with our observations.

The average percentage discrepancies for of κ_x and κ_y from all three methods are $\overline{\Delta\%_x} =$

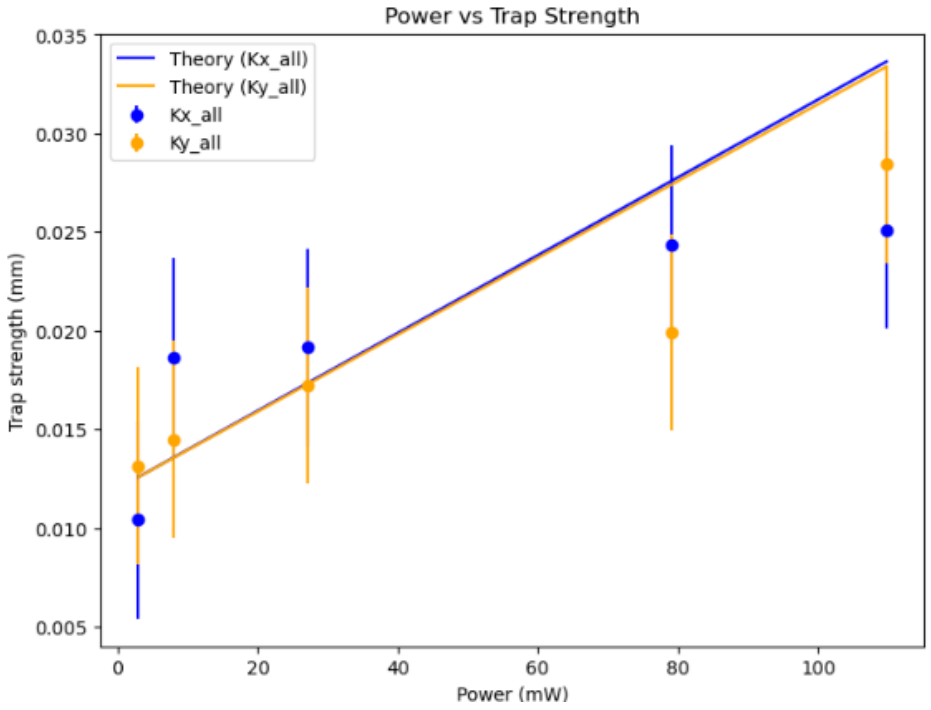

FIG. 6. Plot of the optical trap strength as a function of laser power, in both the x and y directions. The error bars represent the standard deviation of the trap strength measurements, obtained from 5 measurements. The Mie-approximation representing the linear relationship between trap strength and laser power in Equation 13 is then fit to the data to establish potential linearity. The uncertainty in the trap strength at various laser power settings, represented by the error bars, was established by independently calibrating the laser power utilizing a power meter. Graphs of both the x and y dimensions were superimposed on one another to show the invariance of the theory (the linear plots) across both dimensions, and the deviation of the κ_x and κ_y points from the theory, and from each other.

4.62% and $\overline{\Delta\%_y} = 12.30\%$ respectively. We obtained chi-squared values of: $\chi_x^2 = 14.8$ and $\chi_y^2 = 20.67$. The percentage differences between the values for x are relatively small. On the other hand, the percentage differences between the values for y are larger. The chi-squared values indicate a low agreeability to the theoretical approximations [10, 12]. However our data indicates a good approximation to theory from visual analyses of all fitted plots. This is due to experimental sources of error, and will be focused on in the *Discussion*. See Table I for all measured experimental values.

We analyzed the auto-correlation function (ACF) to study the trapped particle's dynam-

ics and trapping environment properties. Figure 5 confirmed the expected Brownian motion behavior, with the function decaying exponentially, consistent with Equation 4. We observed no correlation between signals at different times, and fluctuations were proportional to $\frac{1}{\sqrt{N}}$ as expected (see *Theory*). These results confirm the trapped particle experienced a simple harmonic oscillator potential.

Finally, we investigated the relationship between trap strength and laser power by plotting the force constants κ_x and κ_y against varying values of laser power (Table II). We plotted both spatial coordinates onto one as the linear relationship should be similar across both coordinates. Figure 6 shows a correlational linear relationship consistent with the Mie-scattering approximation [1], which was what the data was fitted against (Equation 13). Comparing against literature, we find that our values for the force constants per laser power fall within the range of typical values [10, 12]. This further substantiates our experimental setup and methods.

DISCUSSION

The position histogram of the polystyrene spheres showed a Gaussian distribution, which is characteristic of Brownian motion, as seen in Figure 3. This indicated that the data was consistent with the expected theoretical distribution [12]. The distributions were slightly skewed to the left and right for x and y respectively, which may have been caused by issues with the laser alignment into the objective, or software bias. While the probability distribution method is less sensitive to external forces acting on the bead, it requires a large number of observations to obtain an accurate measurement. Non-uniformities in the trap, such as spatial variations in the laser intensity, scratches on the camera filter, or bead size variation, may affect the accuracy of the method. This was accounted for in averaging radius, calculated to be $3.3 \pm 0.3\mu$m.

The potential energy plots seen in Figure 4 were observed to be at a minimum at the trap center and rose rapidly as the distance from the trap center expanded, based on 3. This behavior aligns with the harmonic oscillator potentials described in Equations 1 and 2, suggesting that the trapped particle exhibits the characteristics of a simple harmonic oscillator. Our results showed that increasing laser power results in a deeper potential well and a steeper potential energy curve. This is consistent with theoretical predictions and

previous experimental studies[12]. We observed outliers in the points plotted, which could be limitations due to non-idealities in the optical setup or external forces. The force applied is assumed to be constant over time, and the method assumes that the bead is not subject to any external forces. In reality, fluctuations in the laser beam or the surrounding medium may cause the force on the bead to vary over time, and hydrodynamic drag and other external forces may act on the bead [12]. These factors can introduce errors into the measurement of trap strength using the potential energy method.

Our analysis of the trapped particle's motion using the autocorrelation function revealed its time-dependent behavior and characteristic timescale, as shown in Figure 5. We observed an increase in decay time with laser power, indicating a slower and more constant motion as in Equation 4. The presence of oscillations and long-time tails in the autocorrelation function implies potential non-linearities in the trapping or other motion modes. Variations in trap stiffness and non-Gaussian particle motion due to external factors may limit analysis accuracy. Despite these limitations, the autocorrelation function proves useful, with data adjusted for offsets before calculations to account for these issues.

Our research confirms that trap strength increases with laser power, aligning with theoretical predictions [12]. By adjusting laser power, researchers can customize the strength of optical traps for specific experimental needs. However, our study's limitations should be acknowledged, including variations in the trapping environment and the potential for differences in particle behavior due to size, shape, or refractive index, which may limit the generalizability of our findings.

The consistency of percentage uncertainties across all three methods indicate a high precision. The chi-squared values indicate deviation from theory, and suggest the presence of systematic errors (I). Microvibrations, scratched lenses, laser-objective alignment drift (due to faulty joints), particle size, noise (contributes to setup bias), calibration, temperature fluctuations, and inadequate camera frame rate are all examples of systematic errors that can corrupt experimentation. If the camera's frame rate is too low, it may not capture the rapid motion of trapped particles, leading to inaccurate results. Despite these limitations, our study offers valuable insights into optical trapping physics, and builds on the foundations laid by those such as Ashkin [10].

CONCLUSION

In conclusion, our study investigated optical trapping principles and applications using various experimental methods, finding consistency with theoretical predictions and previous studies. We observed Brownian motion behavior, trap strength increasing with laser power, and emphasized the importance of careful calibration and measurement procedures to minimize errors. Future research could explore non-Gaussian particle motion, more complex systems, and further investigate limitations and errors to improve accuracy and precision. It is crucial to understand the underlying principles and experimental apparatus for accurate interpretation of optical trapping results.

ACKNOWLEDGMENTS

We would like to thank K. Winther, D. Lister, H. Brar, B. Mandaher, my partner A. Schimmer, and the professor, Dr. Haljan for their invaluable assistance throughout this course. We would also like to thank Dr. Haljan's dog for being a source of joy on especially arduous experimentation days.

† vsunderr@sfu.ca

[1] T. Tlusty, A. Meller, and R. Bar-Ziv, "Optical gradient forces of strongly localized fields," *Phys. Rev. Lett.* **81**, 1738–1741 (1998).

[2] S. P. Smith S. R. Bhalotra, A. L. Brody, B. L. Brown, E. K. Boyda, and M. Prenetiss, "Inexpensive optical tweezers for undergraduate laboratories", *Am. J. Phys.* **67**, 26–35 (1999).

[3] K. Berg-Sørensen and H. Flyvbjerg, "Power spectrum analysis for optical tweezers," *Rev. Sci. Instrum.* **75**, 594–612 (2004).

[4] K. C. Neuman and A. Nagy, "Single-molecule force spectroscopy: optical tweezers, magnetic tweezers and atomic force microscopy," *Nature Methods*, vol. 5, no. 6, pp. 491–505, 2008.

[5] M. D. Wang, H. Yin, R. Landick, J. Gelles, and S. M. Block, "Stretching DNA with optical tweezers," *Biophys. J.* **77**, 3163–3171 (1999).

[6] V. Bormuth, A. Jannasch, M. Ander, C. van Kats, C. van der Vis, A. M. Schäfer, G. J. L. Wuite, and E. J. G. Peterman, "Optical trapping of coated microspheres," *Journal of Physics: Condensed Matter*, vol. 19, no. 16, p. 165211, 2007.

[7] F. Reif. *Fundamentals of Statistical and Thermal Physics*, Waveland Press Inc. 560-575 (1965).

[8] D. G. Grier, "A revolution in optical manipulation," *Nature* **424**, 810–816 (2003).

[9] A. Ashkin, "History of optical trapping and manipulation of small-neutral particle, atoms, and molecules," *IEEE J. Sel. Top. Quantum Electron.* **12**, 25–42 (2006).

[10] A. Ashkin, J. M. Dziedzic, J. E. Bjorkholm, and Steven Chu, "Observation of a single-beam gradient force optical trap for dielectric particles," *Optics Letters*, vol.11, Issue 5, pp. 288-290 (1986).

[11] J. Bechhoefer and S. Wilson, "Faster, cheaper, safer optical tweezers for the undergraduate laboratory," *Am. J. Phys.* **70**, 393–400 (2002).

[12] P. H. Jones, O. M. Maragò, and G. Volpe, *Optical Tweezers: Principles and Applications*, 1st ed. (Cambridge University Press, 2015).